Functional connectivity predicts changes in attention observed across minutes, days, and months

Monica D. Rosenberg[a,b,1], Dustin Scheinost[c,d,e,f], Abigail S. Greene[f], Emily W. Avery[b], Young Hye Kwon[b], Emily S. Finn[g], Ramachandran Ramani[h], Maolin Qiu[c], R. Todd Constable[c,f,i], and Marvin M. Chun[b,f,j]

[a]Department of Psychology, University of Chicago, Chicago, IL 60637; [b]Department of Psychology, Yale University, New Haven, CT 06520; [c]Department of Radiology and Biomedical Imaging, Yale School of Medicine, New Haven, CT 06510; [d]Child Study Center, Yale School of Medicine, New Haven, CT 06510; [e]Department of Statistics and Data Science, Yale University, New Haven, CT 06520; [f]Interdepartmental Neuroscience Program, Yale University, New Haven, CT 06520; [g]Section on Functional Imaging Methods, Laboratory of Brain and Cognition, National Institute of Mental Health, Bethesda, MD 20892; [h]Department of Anesthesiology, University of Florida College of Medicine, Gainesville, FL 32610; [i]Department of Neurosurgery, Yale School of Medicine, New Haven, CT 06510; and [j]Department of Neuroscience, Yale School of Medicine, New Haven, CT 06510

Edited by Michael I. Posner, University of Oregon, Eugene, OR, and approved January 6, 2020 (received for review July 17, 2019)

The ability to sustain attention differs across people and changes within a single person over time. Although recent work has demonstrated that patterns of functional brain connectivity predict individual differences in sustained attention, whether these same patterns capture fluctuations in attention within individuals remains unclear. Here, across five independent studies, we demonstrate that the sustained attention connectome-based predictive model (CPM), a validated model of sustained attention function, generalizes to predict attentional state from data collected across minutes, days, weeks, and months. Furthermore, the sustained attention CPM is sensitive to within-subject state changes induced by propofol as well as sevoflurane, such that individuals show functional connectivity signatures of stronger attentional states when awake than when under deep sedation and light anesthesia. Together, these results demonstrate that fluctuations in attentional state reflect variability in the same functional connectivity patterns that predict individual differences in sustained attention.

sustained attention | attention fluctuations | individual differences | functional connectivity | predictive modeling

As anyone who has struggled to sit through an esoteric film or reached the end of a paragraph without comprehending its content recognizes, we do not sustain a continuous level of attention at every point in time. Rather, we are frequently distracted by our external environment and our own internal thoughts, and our level of focus fluctuates—intentionally or not (1)—with factors including mindlessness, motivation, resource allocation, and arousal (2).

Functional MRI (fMRI) studies in humans have linked these moment-to-moment attention fluctuations to ongoing activity in large-scale brain networks, including the default mode, dorsal attention, and salience networks (3–8). A growing body of work has also related changes in functional connectivity measured with fMRI and intracranial electroencephalography to changes in attentional and cognitive states (9–14). (Functional connectivity is measured as the statistical dependence between neuroimaging-signal time series in spatially distinct brain regions.) Functional connectivity changes have also been related to changing states of consciousness (15–17). The degree to which functional connectivity dynamics reflect cognitive state dynamics rather than physiological and measurement noise, however, is still debated (18–22). Furthermore, despite these advances, cognitive neuroscience lacks a comprehensive, quantitative measure of intraindividual differences in sustained attention, or changes in attention over time.

In contrast to the discussions on functional connectivity dynamics, there is growing consensus that models based on individuals' unique patterns of static functional brain connectivity (i.e., their functional connectome) can predict individual differences in abilities, including fluid intelligence (23, 24), working memory (25–27), and attention (28–32). Static functional connectivity differs from dynamic functional connectivity in that it provides a single measure of functional brain architecture using an entire neuroimaging-signal time series. The most extensively validated connectome-based predictive model (CPM), the sustained attention CPM (33), has generalized across six independent datasets to predict individuals' overall sustained attention function from functional connectivity measured during rest and five different tasks (33–37). Derived using a data-driven technique (38), the sustained attention CPM comprises a distributed "high-attention" network of functional connections, or edges, stronger in individuals with better sustained attention function and a "low-attention" network of edges stronger in individuals with worse sustained attention. In other words, previous work shows that the sustained attention CPM, a model based on static functional brain connectivity, predicts individual differences in sustained attention function. These predictions can be generated from either task-based or resting-state functional connectivity.

Do the sustained attention CPM's high- and low-attention networks, which predict a person's overall ability to maintain focus, also reflect fluctuations in attentional state? Evidence does suggest that the sustained attention CPM is sensitive to attention improvements following a pharmacological manipulation. That is, healthy adults given a single dose of methylphenidate, a common attention-deficit hyperactivity disorder treatment, show higher high-attention network strength and lower low-attention network strength than unmedicated controls (34). However, this between-subjects study did not directly test whether changes in

Significance

Sustained attention varies across people and fluctuates over time. Patterns of functional brain connectivity predict a person's overall sustained attention ability, but do they predict changes in attentional state? Here, across five studies, we show that the same functional connections that predict overall sustained attention ability predict attention changes observed over minutes, days, weeks, and months. Furthermore, these functional connections are sensitive to cognitive and attentional state changes induced by anesthesia. Thus, fluctuations in the same functional connections that predict attention in part reflect fluctuations in attentional state.

Author contributions: M.D.R., D.S., R.T.C., and M.M.C. designed research; M.D.R., A.S.G., E.W.A., Y.H.K., R.R., and M.Q. performed research; D.S. and E.S.F. contributed new reagents/analytic tools; M.D.R. analyzed data; and M.D.R. wrote the paper with contributions from all authors.

The authors declare no competing interest.

This article is a PNAS Direct Submission.

Data deposition: The data reported in this paper for Experiment 2 have been deposited in the National Institute of Mental Health Data Archive at https://nda.nih.gov/edit_collection.html?id=2402.

[1]To whom correspondence may be addressed. Email: mdrosenberg@uchicago.edu.

First published February 4, 2020.

attention network strength mirror changes in attentional state, and it remains an open question whether the same functional networks that predict differences in attention between people also predict differences in attention within a single person over time.

Here, in a series of experiments, we ask whether the sustained attention CPM predicts a person's attention task performance—above and beyond predicting their overall level of sustained attention function—during short experimental blocks and fMRI sessions spread across days, weeks, and months. Furthermore, we evaluate the model's sensitivity to cognitive and attentional state changes resulting from pharmacological interventions by comparing task-free functional connectivity before and after the administration of two anesthetics, propofol and sevoflurane, with different mechanisms of action (for reviews, see refs. 39 and 40). Our results replicate findings that the sustained attention CPM generalizes to novel individuals to predict their average sustained attention function and, moreover, demonstrate that the model predicts minute-by-minute, day-by-day, and drug-induced changes in attentional state. Thus, the same neuromarker predicts both inter- and intraindividual differences in sustained attention, and fluctuations in functional connectivity around a person's mean "functional connectome fingerprint" in part reflect fluctuations in behaviorally relevant attentional states.

Results

Experiment 1: Sustained Attention Network Strength Predicts Minute-To-Minute Attention Fluctuations. As a first step, to test whether models predict fluctuations in sustained attention from functional connectivity, we reanalyzed fMRI data from 25 individuals performing a challenging sustained attention task (the gradual-onset continuous performance task, or gradCPT) (41) reported in previous work (33). Each participant performed up to three runs of the gradCPT during fMRI, and each run included four 3-min task blocks separated by 32-s rest breaks. During the task, participants saw city and mountain photographs continuously transitioning from one to the next at a rate of 800 ms/image and were instructed to press a button in response to city scenes (90%) but not to mountain scenes (10%).

Mean gradCPT sensitivity (d') was 2.11 (SD = 0.92). Mean SD of d' across task blocks was 0.50, and mean coefficient of variation (SD divided by the mean) of d' across task blocks was 32%. Individuals' overall d' scores were inversely related to their coefficients of variation ($r_s = -0.83$, $P = 2.09 \times 10^{-6}$) but not to their SD of d' across task blocks ($r_s = -0.22$, $P = 0.28$). Suggesting that changes in d' over time were, to some degree, consistent across participants, performance fluctuations were significantly albeit weakly correlated across individuals (mean pairwise Spearman correlation between participants' d' time series = 0.083, $P = 0.003$ based on 10,000 permutations).

Predictions from task-block connectivity. Do brain-based models trained to predict individuals' average sustained attention function also predict changes in sustained attention performance from one minute to the next? To address this question, we trained models to predict gradCPT performance in a subset of individuals and applied them to task-block data from a novel person to generate a behavioral prediction for each block of gradCPT performance. If the same model predicts differences in attention between individuals and differences in attention in a single person, predicted and observed performance scores should be related within-subject. If, in contrast, the model is only sensitive to a person's overall or average level of task performance, predicted and observed performance scores will not be related within-subject.

To this end, to predict minute-by-minute gradCPT performance from functional connectivity patterns, multiple functional connectivity matrices were generated for each individual using a 268-node whole-brain functional atlas (42): one overall task matrix from data concatenated across task runs, up to 12 task-block matrices from volumes acquired during individual 3-min task blocks, and up to 9 rest-break matrices using volumes acquired during 32-s rest breaks. Next, using leave-one-subject-out cross-validation, connectome-based models were trained to predict d' using $n - 1$ participants' overall task matrices. In every round of cross-validation, the model was applied to each of the held-out individual's task-block matrices to generate block-specific d' predictions. This prediction pipeline replicated that of ref. 33, except that models were applied to the held-out participant's task-block matrices rather than to their overall task matrix (*Methods*).

Previous work confirmed that head motion is not significantly correlated with d' across individuals in this sample (ref. 33 and *Methods*). However, there is a moderate within-subject relationship between mean frame-to-frame head motion and d' across task blocks (mean within-subject $r_s = -0.31$). Thus, the performance of all models in Experiment 1 was evaluated with Spearman partial correlations between predicted and observed block-wise d' scores controlling for mean frame-to-frame head motion.

At the group level, models trained on overall task matrices generalized to predict task block-specific gradCPT performance in unseen individuals (mean within-subject Spearman partial correlation = 0.45, SD = 0.50; $t_{24} = 5.10$, $P = 3.24 \times 10^{-5}$; Fig. 1). Predictions were significant at $P < 0.05$ in 8 of 25 participants based on permutation tests. Importantly, these models, which predict block-specific gradCPT performance, previously generalized to predict participants' mean performance over the course of the entire scan session (33).

Predictions from rest-break connectivity. Task-based functional connectivity measured during brief 3-min task blocks predicts block-specific task performance in individual subjects. Task-free functional connectivity patterns may also reflect transient attentional states. To test this possibility, models trained on 24 participants' overall task matrices were applied to each of the left-out subjects' rest-break matrices to generate a predicted d' score corresponding to each rest break. Thus, the model generated six predictions for participants with two gradCPT runs and nine predictions for participants with three. Because gradCPT performance is not measured during rest breaks themselves, model performance was assessed by correlating predictions with the d' scores from the preceding and following task blocks (controlling for mean frame-to-frame head motion during rest breaks with partial correlation). These models are referred to as the "prebreak" and "postbreak" models, respectively.

Models trained on overall task matrices generalized to predict left-out individuals' performance fluctuations from functional connectivity observed during task-free rest breaks. Model predictions were significantly related to performance during the blocks immediately following breaks (mean within-subject partial $r_s = 0.25$, SD = 0.56; $t_{24} = 2.33$, $P = 0.029$; Fig. 1). However, model predictions were not significantly correlated with performance during the blocks immediately preceding rest breaks (mean within-subject partial $r_s = 0.16$, SD = 0.51; $t_{24} = 1.39$, $P = 0.18$; Fig. 1). Predictions were significantly related to postbreak behavior in 4 of 25 participants and to prebreak behavior in 3 of 25 participants.

As expected, behavioral predictions from task-block connectivity patterns were more accurate than those from rest-break patterns (task-block vs. prebreak: $t_{24} = 2.20$, $P = 0.038$; task-block vs. postbreak: $t_{24} = 1.85$, $P = 0.077$). However, predictions from rest-break functional connectivity were not significantly more correlated with postbreak than prebreak behavior ($t_{24} = 0.48$, $P = 0.63$). In other words, although rest-break models significantly predicted upcoming task performance but not past task performance, postbreak models were not significantly more accurate than prebreak models. This suggests that functional connectivity patterns observed during midtask rest breaks may reflect local attentional state rather than past or future attentional performance alone.

Individual differences in model performance. Task-block models more accurately predicted attention fluctuations in participants with

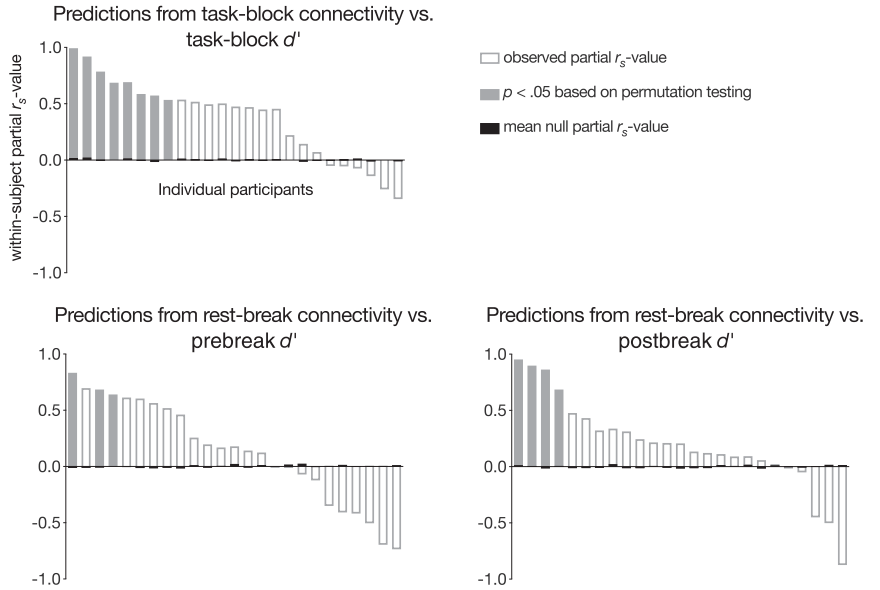

Fig. 1. Within-subject Spearman partial correlations between block-wise d' scores and task-block and rest-break predictions, controlling for task-block or rest-break head motion. Subject-level significance was determined with permutation testing. Group-level significance was assessed with a t test between observed and mean null partial correlations between predicted and observed behavior (task-block model: $P = 3.24 \times 10^{-5}$; prebreak model: $P = 0.18$; postbreak model: $P = 0.029$).

higher coefficients of variation ($r_s = 0.58$, $P = 0.003$). There was a trend such that task-block models also better predicted performance in individuals with lower overall d' values ($r_s = -0.48$, $P = 0.017$), although this relationship does not survive Bonferroni correction for six post hoc comparisons (three models [task-block, prebreak, postbreak] × two behavioral measures [d', coefficient of variation]). Overall d' and d' coefficient of variation values were not significantly related to prebreak or postbreak model accuracy (P values > 0.19).

Predictive network anatomy. Because feature-selection and model-building steps replicated those described in ref. 33, predictive networks are identical to those reported previously. Briefly, across the 25 rounds of leave-one-out cross-validation, networks predicting better d' scores included 1,279 to 1,540 functional connections (mean = 1,426.7, SD = 73.9; "positive networks"), and networks predicting worse d' scores included 1,099 to 1,373 functional connections (mean = 1,251.1, SD = 68.1; "negative networks"). The 757 edges common to all 25 positive networks and the 630 edges common to all 25 negative networks comprise the high-attention and low-attention networks, respectively (Fig. 2). The high- and low-attention networks are distributed across the cortex, subcortex, and cerebellum and are robust to computational lesioning methods that exclude predictive nodes and edges in individual brain lobes and canonical functional networks (33). Thus, the current results demonstrate that the same distributed pattern of functional brain connectivity that predicts interindividual differences in sustained attention also predicts intraindividual differences in attention.

Experiment 2: Sustained Attention Network Strength Predicts Session-To-Session Changes in Attention Task Performance. Experiment 1 used leave-one-subject-out cross-validation (i.e., internal validation) to demonstrate that the same functional networks that predict individual differences in sustained attention are sensitive to fluctuations in attention across 3-min task blocks. Here, we test whether a model defined using the full Experiment 1 dataset, the sustained attention CPM, predicts session-to-session variability in focus in completely new individuals. To this end, we analyzed data collected as an independent group of 49 adults performed 10 min of the gradCPT during two MRI sessions approximately 3 wk apart (45). In this external validation sample, mean d' was 2.29 (SD = 0.77) in session 1 and 2.15 (SD = 1.00) in session 2. Performance scores were correlated across sessions ($r_s = 0.71$, $P = 7.99 \times 10^{-9}$) and did not significantly differ between session 1 and session 2 ($t_{48} = 1.40$, $P = 0.17$). Head motion was not significantly correlated with d' in either session and did not significantly differ between sessions (*Methods*).

Attention predictions. The sustained attention CPM was applied to each participant's session 1 and session 2 gradCPT matrices separately to predict session-specific d' scores. Briefly, sustained attention CPM predictions are generated by inputting the difference between an individual's high-attention network strength and low-attention network strength into a linear model whose coefficients were defined in previous work (33). Model outputs correspond to predicted gradCPT d' scores. In the current sample, predicted d' scores were significantly correlated with true d' scores during the first ($r_s = 0.40$, $P = 0.0051$) and second ($r_s = 0.69$, $P = 4.33 \times 10^{-8}$) imaging sessions, demonstrating robust cross-dataset generalization (Fig. 3*A*). Furthermore, predicted d' was higher for participants' better vs. worse scan session ($t_{48} = 3.51$, $P = 9.87 \times 10^{-4}$), and the session with the higher predicted d' corresponded to the session with the higher observed d' in 33 out of 49 individuals (67.3%; Fig. 3*B*). The difference in d' between participants' first and second gradCPT sessions was also correlated with the difference in predicted d' for these sessions ($r_s = 0.61$, $P = 5.39 \times 10^{-6}$). Thus, the same functional connectivity patterns that predict individual differences in sustained attention reflect subtle within-subject changes in attentional performance, even in a highly reliable task.

Experiment 3: Sustained Attention Network Strength Predicts Week-To-Week Changes in Attention in a Single Individual. We next investigated whether the sustained attention CPM is sensitive to within-subject variability in sustained attention observed over the course of weeks and months. To this end, we analyzed a longitudinal dataset described in previous work (46, 47). This dataset consisted of 30 MRI sessions, each including a run of gradCPT performance, from a single individual (a 56-y-old left-handed male) collected over 10 mo. Across all sessions, the participant's mean gradCPT d' was 2.42 (range = 1.30 to 4.45; SD = 0.85).

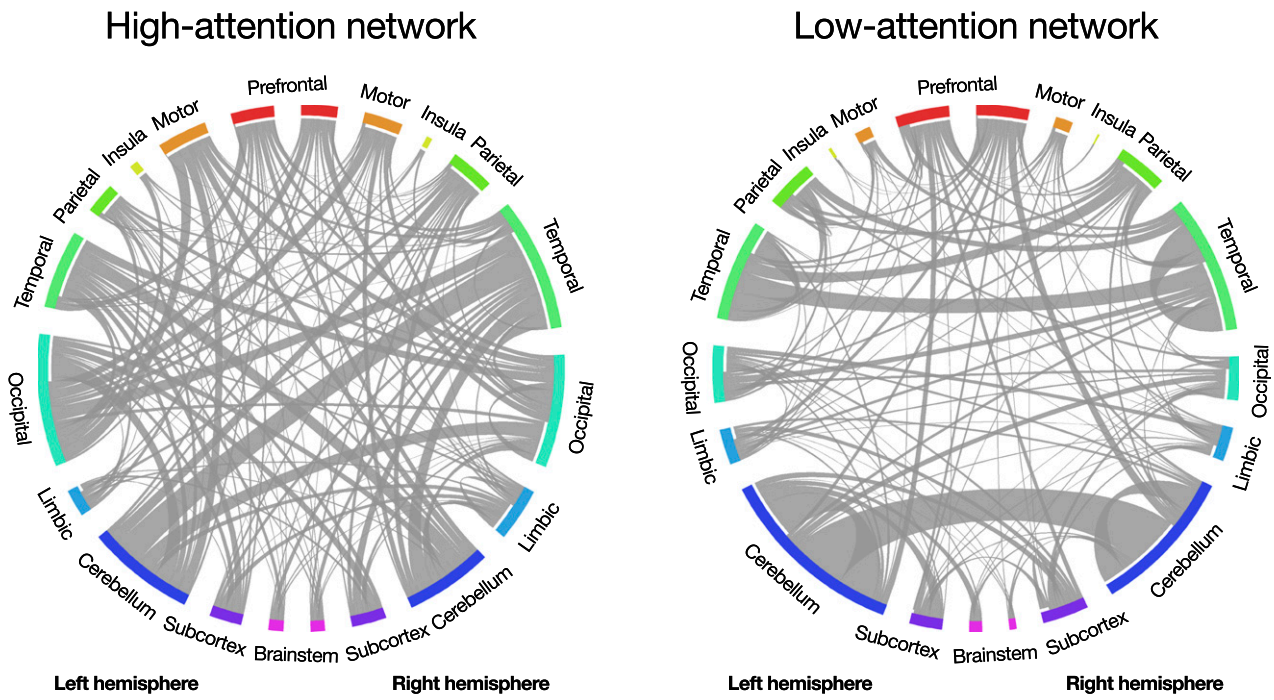

Fig. 2. Functional connections (edges) in the high-attention and low-attention networks (33). Network nodes are grouped into macroscale brain regions; lines between them represent edges. Line width corresponds to the number of edges between region pairs. Created using Circos (43). Adapted with permission from ref. 44.

Performance increased monotonically over the course of the sessions (Spearman correlation between d' and session number; r_s = 0.53, P = 0.003). Due to hardware variability, mean gradCPT trial length ranged from 738 to 800 ms (mean = 778 ms, median = 794 ms, SD = 24.8 ms), and there was a nonsignificant monotonic relationship between trial length and d', such that performance was numerically higher on gradCPT runs with a slower stimulus-presentation rate (r_s = 0.28, P = 0.14). Mean frame-to-frame head motion did not significantly correlate with d' across sessions (r_s = 0.20, P = 0.28).

Trait-like attention prediction. We first validated the sustained attention CPM by applying it to predict this highly sampled individual's average gradCPT performance, a trait-like measure of sustained attention abilities. When the model was applied to the participant's mean gradCPT functional connectivity matrix across all 30 sessions, predicted d' was remarkably similar to true average performance (predicted mean d' = 2.37 vs. observed mean d' = 2.42). Although standard statistical tests cannot be applied to assess the significance of this single observation, we compared prediction error (i.e., the absolute difference between observed and predicted mean d' values) to a distribution of null-model prediction-error values. The null distribution was generated by redefining a CPM in Experiment 1 using shuffled behavioral scores 1,000 times and applying each null model to the Experiment 3 participant's mean gradCPT functional connectivity matrix. The observed prediction error (0.054) was smaller than 91.6% of null-model prediction-error values.

The observed prediction error was also smaller than the absolute prediction error of the task-based general linear model for all but one participant in ref. 33, despite the fact that the current dataset is an external validation sample collected with different scan parameters (Fig. 4*A*). The lower absolute error here may arise because the current dataset includes more fMRI data per individual (165 min vs. 36 min) and/or reflects a more trait-like estimate of the participant's overall ability to maintain focus. Furthermore, suggesting that prediction accuracy is not driven by regression to the training set mean, predicted mean d' is closer to the participant's true mean d' than it is to the average d' of all training subjects (|predicted mean d' − observed mean d'| = 0.054; |predicted mean d' − training set mean d'| = 0.26).

State-like attention predictions. We next applied the sustained attention CPM to data from each scan session separately to generate session-specific d' predictions. Predictions were positively correlated with observed d' values (r_s = 0.42, P = 0.02; Fig. 4*B*), which reflect both state-like and trait-like aspects of sustained attention. Predictions remained significant when controlling for mean trial duration and session number with partial correlation (partial r_s = 0.39, P = 0.04). As a post hoc analysis, given that mean trial duration was non-normally distributed, we divided runs based on a median split of trial duration and assessed predictive power separately in each half. Predictions were significant in the 15 runs with faster trials (r_s = 0.66, P = 0.0095) but nonsignificant in the 15 runs with slower trials (r_s = 0.04, P = 0.88). Thus, the same networks that predict individual differences in attention, block-to-block fluctuations in

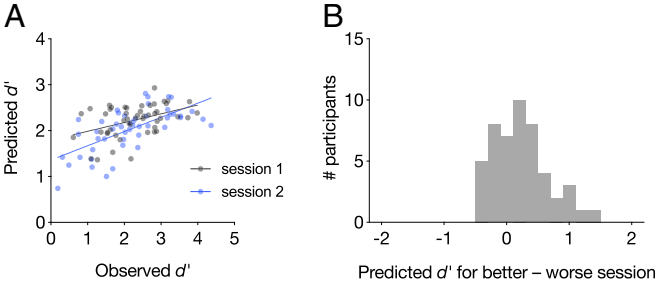

Fig. 3. (*A*) The sustained attention CPM generalized to predict gradCPT performance during two neuroimaging sessions. Each participant is represented with one gray dot corresponding to session 1 performance and one blue dot corresponding to session 2 performance. (*B*) Difference in predicted performance for each person's better and worse task sessions. Values greater than zero indicate that the model correctly predicted a higher score for the better session.

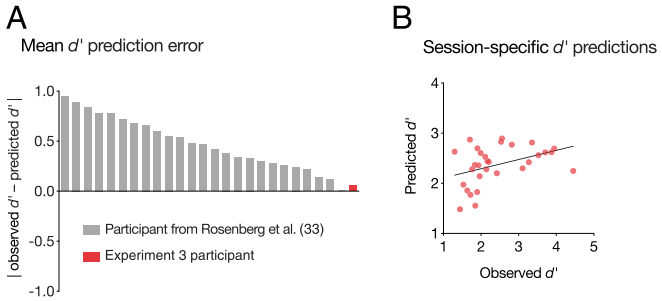

Fig. 4. The sustained attention CPM generalized to predict an individual's mean gradCPT performance (*A*) as well as day-to-day fluctuations around this mean (*B*).

an internal validation dataset, and session-to-session variability in an independent 49-person sample capture mean performance and session-to-session fluctuations in a dense longitudinal phenotyping sample.

Within-subject model comparison. In Experiments 1 to 3, we applied the publication-preregistered sustained attention CPM to data collected from the same individuals at different points in time. This allows us to ask whether the same pattern of functional brain connectivity that predicts differences in sustained attention function between individuals also predicts variations in attentional state. However, two open questions remain. First, would a model trained to predict attention in one individual better capture changes in that person's sustained attention performance over time? Second, would such a model generalize to a novel sample to predict individual differences in sustained attention?

To address these questions, we trained a new CPM using the Experiment 3 dense phenotyping sample with the approach described in *Connectome-based predictive modeling* under *Methods*. (We elected to use this sample as it includes the most data per individual of the studies included here.) Specifically, we trained a model using data from 29 of the participant's 30 fMRI sessions and applied it to data from the left-out session to predict that session's gradCPT performance. We repeated this process leaving each session out once and then related observed and predicted session-specific d' values with Spearman correlation to assess predictive power.

This new CPM (the "within-subject CPM") predicted session-specific task performance ($r_s = 0.46$, $P = 0.005$ based on 1,000 permutations). By comparison, the sustained attention CPM—which was trained to predict individual differences in gradCPT performance in an independent group of people—showed similar predictive power when applied to these data ($r_s = 0.42$, $P = 0.02$). Predictive power of the two models did not significantly differ (Steiger $z = 0.47$, $P = 0.64$), suggesting the intriguing possibility that models trained to predict individual differences in attention capture attention fluctuations just as well as participant-specific models trained to predict attention changes. However, training data were not equated for factors including degrees of freedom and behavioral variability, and this is a case study of a single participant-specific model. Thus, future work is needed to directly compare the predictive power and generalizability of models trained to predict inter- vs. intraindividual differences in attention.

To ask whether a model that predicts changes in one person's attentional performance over time generalizes to predict attentional abilities in a novel sample, we next applied the within-subject CPM to task data from the Experiment 1 dataset ($n = 25$). The resulting predictions were significantly correlated with observed d' scores ($r_s = 0.68$, $P = 2.65 \times 10^{-4}$). In other words, a model trained to predict within-subject differences in gradCPT performance generalized to a completely independent sample to predict individual differences in performance.

Characterizing the anatomy of the within-subject CPM revealed significant overlap with the original sustained attention CPM's high- and low-attention networks. The network that predicted better gradCPT performance in the Experiment 3 participant included 211 functional connections. Of these, 19 were included in the sustained attention CPM's high-attention network ($P = 2.87 \times 10^{-8}$), whereas only 3 were included in the low-attention network ($P = 0.51$). The network that predicted worse gradCPT performance in the Experiment 3 participant included 172 functional connections. Of these, 11 appeared in the sustained attention CPM's low-attention network ($P = 5.88 \times 10^{-5}$), and none appeared in the high-attention network. Therefore, as expected, there is significant overlap between both networks predicting better performance and both networks predicting worse performance. There is no more overlap than would be expected by chance between networks predicting better performance in one model and worse performance in the other.

Experiment 4: Propofol Modulates Sustained Attention Network Strength. The sustained attention CPM captures within-subject changes in sustained attention observed in data collected minutes, days, weeks, and months apart. These attentional state changes likely result from fluctuations in internal and external distraction, as well as variability in neurocognitive states such as motivation and sleepiness. To characterize the sensitivity of the sustained attention CPM to a completely different kind of attentional state change—one induced by pharmacological manipulation—we analyzed MRI data collected from 21 adults while awake (eyes-closed rest) and under deep sedation with propofol in the same imaging session (dataset described in ref. 48). End-tidal CO_2, a measure of carbon dioxide concentration at the end of an exhalation, heart rate, and head motion did not significantly differ between the propofol and awake conditions (ref. 46 and *Methods*). Mean blood pressure was lower in the propofol condition but fell within the autoregulatory range (48).

As predicted, participants showed functional connectivity signatures of stronger attention—higher high-attention network strength and lower low-attention network strength—when awake than when under deep sedation (high-attention network: $t_{20} = 4.53$, $P = 2.03 \times 10^{-4}$ [effect larger than effects on 93.07% of same-size random networks]; low-attention network: $t_{20} = -7.71$, $P = 2.05 \times 10^{-7}$ [effect larger than effects on 99.98% of same-size random networks]; Fig. 5*A*). In other words, the sustained attention CPM was sensitive to an anesthesia-induced attentional and cognitive state change.

Demonstrating the relative specificity of propofol effects to a priori attention networks, the low-attention network showed a larger propofol effect than did any canonical resting-state network (defined in ref. 23). The high-attention network showed a larger propofol effect than all but within-default network connections, medial-frontal network–frontoparietal network connections, and visual I network–visual association network connections (Fig. 5*B*).

Experiment 5: Sevoflurane Modulates Sustained Attention Network Strength. We replicated effects of anesthesia on the sustained attention CPM's high- and low-attention networks using an independent sample of 11 adults scanned while awake, under light anesthesia with sevoflurane, and recovering from anesthesia (dataset described in ref. 49). Head motion, heart and respiratory rates, end-tidal CO_2, and O_2 partial pressure, a measure of blood oxygen saturation, did not significantly differ between the awake and sevoflurane conditions (ref. 48 and *Methods*). Although systolic, diastolic, and mean blood pressure decreased under anesthesia, these changes fell within the autoregulatory range and were unlikely to have resulted in hemodynamic changes (49).

As with propofol, participants showed higher high-attention and lower low-attention network strength in the awake than the

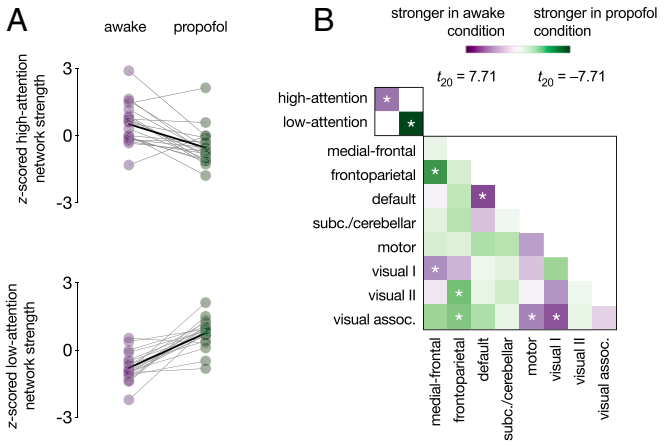

Fig. 5. Effects of propofol on functional network strength. (*A*) High-attention and low-attention network strength during the awake and deep-sedation conditions. Network strength values were *z*-scored within graph for visualization. Individual dots represent individual participants, gray lines represent individual participant network strength change, and solid black lines indicate group mean change. (*B*) Differences in within-network and between-network strength (i.e., summed functional connectivity) during the awake and deep-sedation conditions. Low-attention network strength differed by condition more than any network pair in the lower right matrix; high-attention network strength differed more than 33/36 pairs. *$P < 0.05/38$.

anesthesia condition (high-attention network: $t_{10} = 2.15$, $P = 0.057$ [effect larger than effects on 85.15% of same-size random networks]; low-attention network: $t_{10} = -3.37$, $P = 0.0071$ [effect larger than effects on 96.32% of same-size random networks]; Fig. 6*A*). High-attention network strength was higher during the awake than the recovery scan ($t_{10} = 2.27$, $P = 0.047$) and did not significantly differ between the anesthesia and the recovery scans ($t_{10} = -0.57$, $P = 0.58$). Low-attention network strength was not significantly different during the awake and recovery scans ($t_{10} = -1.56$, $P = 0.15$), but there was a trend such that it was lower during the recovery than the anesthesia scan ($t_{10} = -2.14$, $P = 0.058$). Whole-brain analyses revealed stronger connectivity between the medial-frontal and visual I networks and the motor and visual association networks during the awake than the anesthesia condition. Connectivity between the frontoparietal and visual association networks was significantly stronger during the anesthesia than the awake condition (Fig. 6*B*).

Network strength as a function of state change. Propofol and sevoflurane are different anesthetic agents with different pharmacodynamic effects. Whereas participants in the propofol study did not respond to verbal call during the anesthesia condition (Experiment 4), participants in the sevoflurane study were only under light anesthesia (Experiment 5). To characterize relationships between the degree of anesthesia-induced cognitive and attentional state change and attention network strength, we generated a pseudo-dose–response curve by collapsing data across studies. State affected high-attention ($b = -0.57$, SE = 0.15, $F[3,48.9] = 9.61$, $P = 4.29 \times 10^{-5}$) and low-attention ($b = 0.91$, SE = 0.14, $F[3,2.0] = 24.64$, $P = 0.039$) network strength, such that high-attention network strength systematically decreased and low-attention network strength systematically increased as state changes became more dramatic (Fig. 7).

Discussion

Each person has a unique pattern of functional brain connectivity, that, like a fingerprint, distinguishes them from a group (23, 50). Unlike a fingerprint, however, this pattern predicts cognitive and attentional abilities (31, 51) and changes on multiple time scales (i.e., minutes, hours, days, development). Are these changes meaningful—that is, do they reflect behaviorally relevant changes in cognitive and attentional states?

Here, we tested whether a publication-preregistered model, the sustained attention CPM, predicts both trait-like and state-like measures of sustained attention. An internal validation (i.e., leave-one-subject-out) approach first revealed that functional connectivity patterns observed during 3-min task blocks and 32-s rest breaks predict individuals' block-specific task performance (Experiment 1). In other words, the same models that predicted participants' average task performance in previous work (33) were also sensitive to block-to-block fluctuations in performance. When applied to a 49-person external validation sample, a model defined using the full Experiment 1 dataset—the sustained attention CPM—not only predicted participants' task performance during two fMRI sessions but also predicted which session had better performance and which session had worse (Experiment 2). Moreover, when the sustained attention CPM was applied to data from one individual's 30 fMRI sessions, the prediction based on his average functional connectivity pattern reflected his average task performance and predictions based on session-specific patterns reflected session-specific task performance (Experiment 3). Finally, the sustained attention CPM's high- and low-attention networks were modulated by sevoflurane and propofol, such that functional connectivity signatures of better attention were observed when individuals were awake than when they were under light anesthesia or deep sedation (Experiments 4 and 5). Together, these findings demonstrate that behaviorally relevant attentional states are reflected in functional connectivity patterns calculated from less than 30 s of rest data; that, when averaged over many scan sessions, functional connectivity patterns provide highly accurate predictions of average sustained attention function; and that the same functional connections that vary with sustained attention across individuals also change with attentional state within individuals.

The sensitivity of the sustained attention CPM to within-subject state changes suggests that the same functional brain architecture that varies with differences in attention function between people also varies with differences in attention function within individuals over time. In the dense phenotyping sample from Experiment 3, the sustained attention CPM captured these

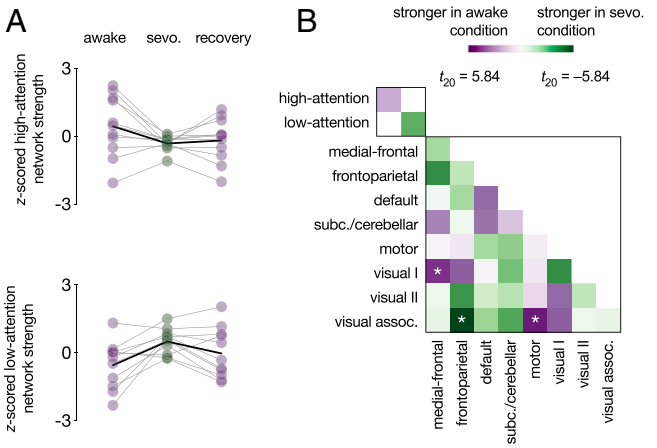

Fig. 6. Effects of sevoflurane (sevo.) on functional network strength. (*A*) High-attention and low-attention network strength during the awake (preanesthesia), sevoflurane, and recovery (postanesthesia) conditions. Network-strength values were *z*-scored within graph for visualization. Individual dots represent individual participants, gray lines represent individual participant network strength change, and solid black lines indicate group mean change. (*B*) Differences in within-network and between-network strength (i.e., summed functional connectivity) during the awake (preanesthesia) and sevoflurane conditions. *$P < 0.05/38$.

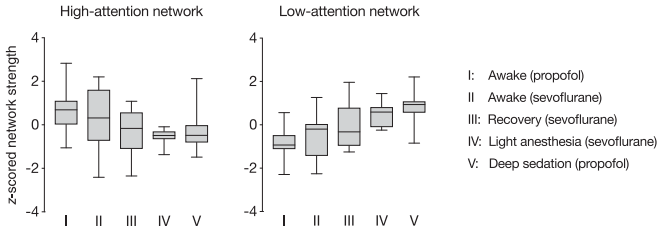

Fig. 7. "Dose–response" curve relating attention network strength to the intensity of state changes across two datasets. Raw network strength values (summed Fisher *z*-transformed correlation coefficients) were normalized within the high-attention network and low-attention network plots separately. Boxes extend from the 25th to 75th percentiles and whiskers from the minimum to maximum values. Horizontal lines correspond to group medians. State changes were most pronounced in the "Deep sedation (propofol)" condition, in which participants were under deep sedation and did not respond to verbal call. Effects of anesthesia were less pronounced in the "Light anesthesia (sevoflurane)" condition and lesser still in the "Recovery (sevoflurane)" condition. Preanesthesia conditions, "Awake (propofol)" and "Awake (sevoflurane)," are equivalent to task-free resting-state scans.

within-subject state changes just as well as a model expressly trained to predict session-specific performance in that sample (Experiment 3). That is, a model trained using data from 29 fMRI sessions from a single participant to predict task performance during a left-out 30th session did not significantly outperform a model trained using data from 25 completely independent individuals. Although this result reflects a single case study and so should be considered preliminary, it suggests that models tailored to a single subject may offer only modest benefits to predictive power when compared with models trained on different subjects. Looking ahead, additional work can test whether models trained to predict individual differences in other cognitive processes also capture within-subject changes in those processes and characterize the relative benefits of participant-specific vs. participant-general models.

The current work aligns with a growing body of evidence that changes in ongoing attention and cognition are reflected in changes in functional connectivity. In particular, functional connectivity dynamics measured with fMRI, particularly in the default mode and dorsal attention networks, mirror changes in task state (13, 52), task performance (10, 11, 14, 53), and self-reported mind wandering (12, 54, 55). Furthermore, a recent intracranial electroencephalography study in humans revealed that default and dorsal attention network activity showed greater lagged anticorrelation during periods of better attention task performance and that dorsal attention activations preceded default mode deactivations (9). Complementing these findings, our results demonstrate that the same functional networks that predict individual differences in attention in novel individuals also predict attentional states specific to task blocks, fMRI sessions, and states of consciousness induced by anesthesia. Furthermore, they suggest that attentional state-relevant dynamics are not constrained to an a priori set of canonical functional networks (e.g., the default mode, dorsal attention, and salience networks, which do not dominate the sustained attention CPM's high- and low-attention networks) (33) but rather span a distributed set of cortical, subcortical, and cerebellar brain regions (Fig. 2).

At the same time as evidence for behaviorally meaningful functional connectivity dynamics accumulates, work shows that functional connection reliability is poor when measured in short time windows (even up to 36 min of data from a single fMRI session) (56) and that dynamics arise due to sources including motion and sampling variability (57). How do we resolve these discrepant observations? One possibility is that attentional state-specific functional connectivity patterns have been previously characterized as noise. That is, attention changes over multiple time scales, and these changes are likely missed by analyses that group task states regardless of behavioral performance or average performance over long periods of time. A corollary to this suggestion is that functional connectivity patterns averaged over long periods of time and multiple fMRI sessions better approximate a person's "true" connectome and better predict behavior in part because they sample a wider range of a person's possible cognitive and attentional states. Importantly, we are not discounting the serious and well-documented effects of physiological and measurement noise on functional connectivity measured at short time scales. Rather, we suggest that a person's attentional state is another statistically significant source of variability in data-driven functional networks that predict attention. (Simultaneously, networks that predict other processes such as emotional reactivity may fluctuate with changes in these states as well.) In the future, multisession, multitask fMRI samples and high-frequency behavioral sampling (e.g., ongoing task performance, pupillometry) can help disentangle the contributions of multiple sources of functional connectivity dynamics.

At first glance, the finding that functional network connectivity predicts moment-to-moment and day-to-day differences in attention stands in apparent contrast to work showing that the organization of canonical functional brain networks reflects stable individual differences rather than task states or day-to-day variability (58). However, the results are not incongruous. First, Gratton et al. (58) characterized the topography of canonical networks such as the default and dorsal attention networks, whereas we consider the strength of a distributed set of functional connections selected to predict behavior with a data-driven approach. More importantly, however, Gratton et al. found that, although task states and fMRI sessions are not dominant sources of variability in functional network organization, they do have significant effects. Thus, it is possible that collapsing across attentional states within broader task states obscures behaviorally relevant differences in network organization and that characterizing networks during distinct periods of successful and unsuccessful task performance could magnify these small but significant effects. Future work characterizing the effects of task challenges and pharmacological interventions (extrinsic state manipulations) as well as attention fluctuations (intrinsic state manipulations) on functional network organization and connectivity patterns will further inform the sources of variability around each individual's average functional connectome fingerprint.

Together, the current work demonstrates that transient functional connectivity patterns reflect local attentional states. However, it remains an open question whether task-based or resting-state functional connectivity patterns predict changes in attention over longer periods of time, such as development and aging. Looking ahead, testing the sensitivity of connectome-based models to within-subject changes in attentional and cognitive abilities over years and decades can inform the common and distinct functional architecture of these processes across the lifespan (59). Furthermore, building new models to predict developmental trajectories in abilities and behavior can provide insights into the ways in which functional brain organization reflects risk for or resilience to impairments such as attention-deficit hyperactivity disorder, potentially informing early treatments or interventions.

In sum, we show that a neuromarker of sustained attention generalizes across five independent datasets to predict individual differences in sustained attention as well as intrinsic and pharmacologically induced attentional states from task-based and task-free functional connectivity. Thus, functional connectivity patterns reflect a combination of trait-like and state-like aspects of sustained attention, and, more broadly, dynamics in functional connectivity in part reflect dynamics in attentional and cognitive states.

Methods

Experiment 1: Sustained Attention Network Strength Predicts Minute-To-Minute Attention Fluctuations.

Participants. Thirty-one right-handed, neurologically healthy adults with normal or corrected-to-normal vision were recruited from Yale University and the surrounding community to perform the gradCPT (41, 60, 61) and rest during MRI data collection (dataset described in ref. 33). The study was approved by the Yale University Institutional Review Board (IRB). All participants provided written informed consent and were paid for their participation. Following exclusion for excessive head motion (>2-mm translation or >3° rotation in all functional runs) or insufficient coverage, data from 25 individuals were submitted to further analysis (13 females, 18 to 32 y, mean = 22.7).

Experimental design. The gradCPT, a test of sustained attention and inhibitory control, was used to assess participants' overall ability to maintain focus and to track their attention fluctuations over time. During the gradCPT, grayscale images of city (90%) and mountain (10%) scenes gradually transitioned from one to the next every 800 ms. Participants were instructed to press a button with their right index finger every time they saw a city scene but not to press to mountain images. Because stimuli were constantly in transition, an iterative algorithm was used to assign button-press responses to trials (33).

Scan sessions began with a high-resolution anatomical image acquisition followed by a 6-min resting-state run, three 13-min, 44-s gradCPT runs, and a second 6-min resting-state run. GradCPT runs included 8 s of fixation followed by four 3-min task blocks interleaved with 32-s rest breaks. Resting-state runs are not analyzed here.

For each task block (3 runs × 4 blocks/run = 12 blocks total), performance was measured with sensitivity (d'), or the inverse of the standard normal cumulative distribution function of the false alarm rate (incorrect presses to mountains) subtracted from the inverse of the standard normal cumulative distribution function of the hit rate (correct presses to cities). Overall gradCPT performance was measured by averaging d' values across blocks.

Imaging parameters and preprocessing. MRI data were collected at the Yale Magnetic Resonance Research Center (MRRC) on a 3T Siemens Trio TIM system using a 32-channel head coil. Functional runs included 824 (task) or 363 (rest) whole-brain volumes acquired using a multiband echoplanar imaging (EPI) sequence with the following parameters: repetition time (TR) = 1,000 ms, echo time (TE) = 30 ms, flip angle = 62°, acquisition matrix = 84 × 84, in-plane resolution = 2.5 mm^2, 51 axial-oblique slices parallel to the anterior commissure–posterior commissure (AC-PC) line, slice thickness = 2.5 mm, multiband 3, acceleration factor = 2. Parameters of the anatomical magnetization prepared rapid gradient echo (MPRAGE) sequence were as follows: TR = 2,530 ms, TE = 3.32 ms, flip angle = 7°, acquisition matrix = 256 × 256, in-plane resolution = 1.0 mm^2, slice thickness = 1.0 mm, 176 sagittal slices. A two-dimensional (2D) T1-weighted image coplanar to the functional images was also collected for registration.

Functional data were analyzed using BioImage Suite (62) and custom Matlab scripts (Mathworks) as described previously (33). Motion correction was performed using SPM8. Linear and quadratic drift, mean signal from the cerebrospinal fluid (CSF) and white matter, and 24 motion parameters were regressed from the data. Global signal was also included as a nuisance regressor to reduce the confounding effects of motion (35, 63). Data were temporally smoothed with a zero mean unit variance Gaussian filter (cutoff frequency = 0.12 Hz).

Preprocessing steps were applied to data concatenated across task runs as well as to data from each task block and rest break separately to maintain independence between block- and break-specific functional connectivity matrices (*Functional connectivity matrix generation*).

Because head motion can confound functional connectivity analyses, five task runs and two rest runs with more than 2-mm head translation or 3° rotation were excluded from analysis. As reported previously, mean frame-to-frame displacement during gradCPT runs and average motion across gradCPT runs did not correlate with d' across individuals ($|r| \leq 0.1$; P values ≥ 0.62) (33).

Functional connectivity matrix generation. Functional network nodes were defined with a 268-node atlas with cortical, subcortical, and cerebellar nodes (42). The atlas was warped from Montreal Neurological Institute (MNI) space into single-subject space via linear and nonlinear registrations between the EPI images, coplanar scan, three-dimensional (3D) anatomical scan, and MNI brain.

To generate whole-brain functional connectivity matrices, the mean fMRI signal time course for each node was calculated by averaging the time courses of its constituent voxels. The Pearson correlation between the average time courses of every pair of nodes was computed and Fisher z-transformed to yield symmetrical 268 × 268 matrices of functional connections, or edges.

To test whether the same functional networks that predict individual differences in attention also predict attention fluctuations, we measured participants' overall pattern of functional connectivity during task engagement as well as their connectivity patterns during shorter intervals over the course of the task. To this end, for each participant, we calculated 1) a single overall task matrix from data concatenated across task runs, excluding volumes collected during rest breaks; 2) up to 12 task-block matrices from volumes acquired during individual task blocks; and 3) up to 9 rest-break matrices using volumes acquired during individual rest breaks (starting 6 s after break onset and ending 3 s before the onset of the upcoming task block to reduce the influence of task-related stimulus processing on rest-break connectivity).

Connectome-based predictive modeling. Previous analyses of these data demonstrated that models based on patterns of functional connectivity observed during the gradCPT—here, the "overall task matrices"—predict individual differences in performance from both task-based and resting-state functional connectivity (33). Furthermore, these same network models generalize to independent datasets to predict measures of attention and inhibitory control including attention-deficit hyperactivity disorder symptoms, stop-signal task performance, and Attention Network Task performance (33–35).

To test whether these same models predict not only differences in attention between individuals but also differences in attention within single individuals over time, we performed a variant of connectome-based predictive modeling (38) using leave-one-subject-out cross-validation. In this pipeline, feature-selection and model-building steps replicate those described in ref. 33, but models are tested on different data from the held-out individual.

First, data from one individual were set aside, leaving overall task matrices and overall d' scores from the remaining 24 participants. Next, robust regression between each edge in the overall task matrices (35,778 total) and d' was performed across subjects. Edges related to behavior at $P < 0.01$ were retained and separated into a positive tail (positive regression coefficients) and a negative tail (negative regression coefficients).

For each participant in the training set, overall strength in the positive and negative tails was calculated by summing their respective connections. The difference in connectivity strength between the tails (positive tail strength–negative tail strength) was used as a predictor in a linear regression of the form $d' = aX + b$. This model differs slightly from the general linear model reported in ref. 33, in which positive and negative tail strength were included as independent predictors. Here, the difference in strength between the tails is used to avoid collinear predictors.

To test whether this model generalized to predict attention fluctuations in previously unseen individuals, it was applied to each of the left-out participant's task-block matrices separately. That is, the difference between positive and negative tail strength was calculated using data from each of the held-out individual's 3-min task blocks. The resulting difference scores (8 for participants with two gradCPT runs and 12 for participants with three) were input in the model to generate a predicted d' value for each task block. Model performance was assessed by computing the Spearman partial correlation between the left-out individual's predicted and observed block-specific d' scores, controlling for mean frame-to-frame head motion in each task block. The prediction pipeline was repeated until every individual had been left out once.

If changes in task-based functional connectivity predict changes in attention, task-free connectivity patterns may also reflect transient attentional states. To test this possibility, the same model was applied to each of the left-out subject's rest-break matrices to generate a predicted d' score corresponding to each rest break (6 for participants with two gradCPT runs and 9 for participants with three). Model performance was assessed by correlating predictions with the d' scores from the preceding and following task blocks since performance is not measured during the breaks themselves. Again, partial correlations were used to control for mean frame-to-frame head motion during rest breaks. These models are referred to as the "prebreak" and "postbreak" models, respectively, throughout the text.

Of note, we used connectome-based predictive modeling as our prediction approach because a primary goal of the current work was to assess whether the same model that predicts individual differences in sustained attention is sensitive to within-subject changes in attentional state. Thus, we applied the exact same model published previously to the current sample and the four other external validation datasets described here. Comparisons between CPM and multivariate techniques, such as support vector regression (38) and partial least squares regression (32), have found numeric but not significant differences in predictive power for sustained attention.

Significance testing. The significance of model predictions was evaluated at both the individual and group levels. To determine whether models significantly predicted fluctuating d' in a single person, block-specific d' scores were shuffled 1,000 times and correlated with model predictions. This process generated two null r_s-value distributions per individual: one of null task-block

predictions and one of null rest-break predictions. The significance of task-block model predictions was calculated as $P = (1 + \text{number of null task-block } r_s \text{ values} \geq \text{observed task-block } r_s)/1{,}001$. The significance of rest-break model predictions was calculated as $P = (1 + \text{number of null rest-break } r_s \text{ values} \geq \text{observed prebreak } r_s)/1{,}001$ and $P = (1 + \text{number of null rest-break } r_s \text{ values} \geq \text{observed postbreak } r_s)/1{,}001$.

The significance of model predictions was also evaluated at the group-level with paired *t* tests comparing observed within-subject r_s values to the mean of each participant's null task-based or rest-break r_s-value distribution. Spearman correlation coefficients were Fisher *z*-transformed before averaging; averaged *z* values were converted back to r_s values for reporting.

Experiment 2: Sustained Attention Network Strength Predicts Session-To-Session Changes in Attention Task Performance.

Participants and experimental design. Ninety-eight individuals (62 female, ages 18 to 35 y, mean = 22.9, SD=4.6) participated in a two-session neuroimaging experiment designed to assess different aspects of attention and memory (45). Ninety participants completed both sessions, which included 10-min resting-state runs (two in session 1 and one in session 2); an Inscapes movie run (one per session) (64); gradCPT, multiple object tracking, visual short-term memory task runs (one per session; order counterbalanced across participants and sessions); and an Attention Network Task run (one in session 2). Participants provided written informed consent in compliance with procedures approved by the Yale University IRB and were paid for their participation.

GradCPT data from the 49 individuals with whole-brain coverage, d' scores within 3 SDs of the group mean, and acceptable levels of head motion (<3 mm maximum displacement and <0.15 mm mean frame-to-frame displacement) during session 1 and session 2 were analyzed here (34 female, ages 18 to 32 y, mean = 23.3, SD = 4.2). For these individuals, fMRI sessions were held approximately 3 wk apart (range = 5 to 133 d, mean = 20.4, SD = 25.1). The number of days separating sessions 1 and 2 did not correlate with gradCPT performance on either day or with the difference between them ($|r_s| < 0.066$, *P* values > 0.65). No other data were tested, and this dataset has not been published previously.

Imaging parameters and preprocessing. MRI data were collected at the Yale MRRC on a 3T Siemens Prisma system using a 64-channel head coil. Functional gradCPT runs included 600 whole-brain volumes acquired using a multiband EPI sequence with the following parameters: TR = 1,000 ms, TE = 30 ms, flip angle = 62°, acquisition matrix = 84 × 84, in-plane resolution = 2.5 mm^2, 52 axial-oblique slices parallel to the AC-PC line, slice thickness = 2.5 mm, multiband 4, acceleration factor = 1. Parameters of the MPRAGE sequence were as follows: TR = 1,800 ms, TE = 2.26 ms, flip angle = 8°, acquisition matrix = 256 × 256, in-plane resolution = 1.0 mm^2, slice thickness = 1.0 mm, 208 sagittal slices.

Data were processed with AFNI (65). Preprocessing steps included the exclusion of three volumes from the start of each run; censoring of volumes in which more than 10% of voxels were outliers; censoring of volumes for which the Euclidean norm of the head motion parameter derivatives exceeded 0.2; despiking; slice-time correction; motion correction; and regression of mean signal from the CSF, white matter, and whole brain as well as 24 motion parameters. Functional images were aligned to their corresponding skull-stripped high-resolution anatomical image via linear transformation, and the anatomical image was aligned to MNI space. For each session, a functional connectivity matrix was defined from gradCPT data as described in Experiment 1.

d' values were not significantly correlated with mean frame-to-frame motion after censoring, maximum motion after censoring, or number of frames censored (session 1: $|r_s| < 0.26$, *P* values > 0.075; session 2: $|r_s| < 0.151$, *P* values > 0.30). Head motion and number of postcensoring volumes did not differ between participants' day 1 and day 2 gradCPT runs, their better and worse gradCPT runs, or their predicted-better and predicted-worse gradCPT runs ($|t_{48}| < 1.32$, *P* values > 0.19).

Attention predictions. The model used for external validation, the sustained attention CPM, was defined using the high-attention and low-attention networks described in *Predictive network anatomy* for Experiment 1. Using data from all 25 participants in the (33) sample, a linear regression of the form $d' = aX + b$ was computed where X = high-attention network strength − low-attention network strength. This model, the sustained attention CPM, was applied, completely unchanged, to each participant's session 1 and session 2 gradCPT matrix to generate two d' predictions. Model performance was assessed by rank-correlating predictions with d' scores across individuals for each session separately. A paired *t* test was applied to compare predictions for participants' better vs. worse session.

Experiment 3: Sustained Attention Network Strength Predicts Week-To-Week Changes in Attention in a Single Individual.

Participant and experimental design. Thirty sessions of MRI data were collected over 10 mo from a single individual (46, 47). Data were acquired at the Yale MRRC on two identically configured Siemens 3T Prisma scanners using a 64-channel head coil. The participant provided written informed consent in accordance with a protocol approved by the Yale University Human Research Protection Program (46).

During each scan session, six ∼6-min task runs and two 6-min, 49-s resting-state fMRI runs (including initial shim time and 8 s of discarded acquisitions) were collected. Tasks included the gradCPT (450 trials/run) as well as an *n*-back task, stop-signal task, card-guessing task, "reading the mind in the eyes" task, and movies task (46). Here, we restrict our analyses to gradCPT data. Attention was operationalized as gradCPT sensitivity (d'). Mean frame-to-frame head motion during gradCPT runs was not significantly correlated with d' across sessions ($r_s = 0.20$, $P = 0.28$).

Imaging parameters and preprocessing. A high-resolution anatomical (MPRAGE) scan was collected during the first session with the following parameters: 208 contiguous slices acquired in the sagittal plane, TR = 2,400 ms, TE = 1.22 ms, flip angle = 8°, slice thickness = 1 mm, in-plane resolution = 1 mm^2, matrix size = 256 × 256. Functional images were collected using a multiband gradient EPI sequence with the following parameters: 75 contiguous slices acquired in the axial-oblique plane parallel to AC-PC line, TR = 1,000 ms, TE = 30 ms, flip angle = 55°, slice thickness = 2 mm, multiband = 5, acceleration factor = 2, in-plane resolution = 2 mm^2, matrix size = 110 × 110 (46).

Imaging data were analyzed using BioImage Suite and custom MATLAB scripts. Motion correction was performed using SPM12. White matter and CSF masks were defined in MNI space and warped into single-subject space using linear and nonlinear transformations. Linear, quadratic, and cubic drift, a 24-parameter motion model, mean signal from CSF and white matter, and mean global signal were regressed from the data. Lastly, data were temporally smoothed with a Gaussian filter (sigma = 1.55, cutoff frequency = 0.121 Hz) (46).

For each session, a functional connectivity matrix was generated from gradCPT data as described for Experiment 1. Due to hardware variability, mean gradCPT trial length ranged from 738 to 800 ms (mean = 778 ms, median = 794 ms, SD = 24.8 ms). Thus, matrices were calculated from the first 330 volumes of every run to account for differences in task duration.

Attention predictions. The sustained attention CPM was applied to the participant's gradCPT functional connectivity matrices to generate session-specific d' predictions. Model performance was assessed by rank-correlating predictions with d' scores across the 30 sessions.

Within-subject model network overlap. To compare the predictive power of the sustained attention CPM to the predictive power of a model trained to predict within-subject changes, we built a new CPM using the Experiment 3 data with the method described in *Connectome-based predictive modeling* for Experiment 1 (*Methods*). Specifically, we used leave-one-session-out cross-validation to predict session-specific gradCPT performance.

To assess the overlap between this new within-subject CPM's component networks and the original sustained attention CPM's high- and low-attention networks, we first retained functional connections that appeared in every round of leave-one-session-out cross-validation. This revealed 211 functional connections in the within-subject network predicting higher d' scores and 172 functional connections in the within-subject network predicting lower d' scores.

The significance of the overlap between the within-subject CPM networks and the sustained attention CPM networks was determined with the hypergeometric cumulative density function, which returns the probability of drawing up to x of K possible items in n drawings without replacement from an M-item population. This was implemented in Matlab as $P = 1 - \text{hygecdf}(x, M, K, n)$, where x is the number of overlapping edges, K is the number of connections in the sustained attention CPM network of interest, n is the number of connections in the within-subject CPM network of interest, and M is the total number of functional connections (edges) in the matrix (35,778).

Experiment 4: Propofol Modulates Sustained Attention Network Strength.

Participants and experimental design. fMRI data were collected from 32 adults while awake (eyes-closed rest) and under deep sedation in accordance with research protocols approved by the Yale University IRB (13 female, ages 19 to 35 y; dataset described in ref. 48). Participants provided written informed consent. After exclusion for excessive head motion (>0.15 mm mean frame-to-frame displacement) in either condition, data from 21 participants remained. Head motion did not differ between awake and deep-sedation conditions (awake: 0.078 ± 0.04 mm, deep sedation: 0.077 ± 0.03 mm; $t_{20} = 0.017$, $P = 0.99$).

Imaging parameters and preprocessing. MRI data were collected at the Yale MRRC on a 3T Siemens Trio TIM system using a 12-channel head coil. Two functional runs collected during both the awake and deep-sedation conditions included 210 whole-brain volumes acquired using an EPI sequence with the following parameters: TR = 2,000 ms, TE = 30 ms, field-of-view (FOV) = 256 × 256 mm^2, flip angle = 90°, matrix size = 64 × 64, 33 AC-PC aligned slices, slice thickness = 4 mm, no gap. After data were collected during the awake condition, propofol was infused intravenously to induce an anesthetized state ("deep sedation") in which participants did not respond to verbal call. During propofol infusion, a high-resolution MPRAGE scan was collected with the following parameters: 176 contiguous sagittal slices, voxel size = 1 mm^3, FOV = 256 × 256 mm^2, TR = 2,530 ms, TE = 3.34 ms, flip angle = 7°. A 2D T1-weighted image with the following parameters was also acquired for the purpose of registration: TR = 300 ms, TE = 2.43 ms, FOV = 256 × 256 mm^2, matrix size = 256 × 256, flip angle = 60°.

Imaging data were analyzed with SPM8 (slice-time correction and motion correction), BioImage Suite (all other preprocessing steps), and custom Matlab scripts. After the first 10 volumes of each functional run were discarded, data were slice time-corrected, motion-corrected, and iteratively smoothed to a smoothness of ∼6 mm full-width half-maximum. Covariates of no interest were regressed from the data including linear and quadratic drift, mean CSF, white matter, and gray matter signal, and a 24-parameter motion model. Data were temporally smoothed with a Gaussian filter (cutoff frequency = ∼0.12 Hz) (48). Time-series data were concatenated across the two runs from the same condition. Functional connectivity matrices were calculated from the awake and propofol conditions as described for Experiment 1.

Network strength comparison. A paired *t* test was used to compare high-attention and low-attention network strength in the awake and deep-sedation conditions. Differences in attention network strength were compared to differences in 10,000 same-size random networks. To further assess the specificity of state-dependent differences, we also compared propofol effects on high-attention and low-attention network strength to propofol effects on functional connectivity within and between the medial-frontal, frontoparietal, default mode, subcortical-cerebellar, motor, visual I, visual II, and visual association networks (23).

Experiment 5: Sevoflurane Modulates Sustained Attention Network Strength.

Participants and experimental design. Neuroimaging data were collected in a single imaging session from 14 adults (7 female, ages 22 to 34 y) while awake, under light anesthesia, and during recovery after anesthesia (dataset described in ref. 49). Data from three participants were excluded from the current analysis due to missing data in one or more scan conditions or excessive head motion during scanning (>0.2 mm frame-to-frame displacement). During the preanesthesia awake condition, participants received pure oxygen through a facemask. During the sevoflurane condition, participants received a mixture of oxygen and sevoflurane (end-tidal concentration 1%, equivalent to 0.5 minimum alveolar concentration). In the postanesthesia recovery condition, participants received pure oxygen again. Conditions were separated by 10-min transition periods, and participants were instructed to keep their eyes closed throughout the study. All participants gave written informed consent, and the Human Investigation Committee of the Yale School of Medicine approved the study protocol. Mean frame-to-frame head motion did not differ between the awake, sevoflurane, and recovery conditions (awake: 0.092 ± 0.06 mm; sevoflurane: 0.077 ± 0.06 mm; recovery: 0.099 ± 0.06 mm; all paired $|t_{10}| < 1.13$, P values > 0.28).

Imaging parameters and preprocessing. MRI data were collected at the Yale MRRC on a 3T Siemens Trio TIM system using a circularly polarized head coil (49). Scan sessions began with a localizer followed by a 2D T1-weighted anatomical scan (TR = 300 ms, TE = 2.43 ms, FOV = 256 mm, matrix size = 256 × 256, flip angle = 60°, 33 axial slices parallel to the AC-PC line, slice thickness = 4 mm, no gap). Functional runs included 210 volumes and were collected during the preanesthesia, anesthesia, and postanesthesia conditions using a T2* sensitive gradient-recalled, single-shot EPI pulse sequence (TR = 2 s, TE = 31 ms, FOV = 256 mm, flip angle = 90°, matrix size = 64 × 64, 33 slices parallel to the bicommissural plane, slice thickness = 4 mm, no gap). High-resolution anatomical (MPRAGE) images were acquired in between the anesthesia and postanesthesia conditions (176 contiguous sagittal slices, slice thickness = 1 mm, matrix size = 256 × 256, FOV = 256 mm, TR = 2,530 ms, TE = 3.34 ms, flip angle = 7°).

Data were analyzed with BioImage Suite. After the first 10 volumes of each functional run were discarded, data were temporally and spatially realigned, corrected to remove slice means and drift, and low pass-filtered at a cutoff frequency of 0.08 Hz. Covariates of no interest were regressed from the data including mean CSF and white matter signal and a six-parameter motion model. Functional images were coregistered to the 2D anatomical image. The 2D anatomical image was then registered to the 3D anatomical image, and the 3D anatomical image was aligned to MNI reference space via nonlinear transformation (49). Functional connectivity matrices were calculated from the awake, sevoflurane, and recovery conditions as described for Experiment 1.

Network strength comparison. Changes in high- and low-attention network strength as well as canonical resting-state networks were assessed as described for Experiment 4.

Network strength as a function of state change. The relationship between cognitive state and normalized attention network strength was assessed with a linear mixed effects model using the lme4 package (66) in R. State, an ordered factor with levels {rest, recovery, sevoflurane, propofol}, was entered into the model as a fixed effect. Intercepts for datasets and participants nested within datasets were included as random effects. The limited-memory Broyden–Fletcher–Goldfarb–Shanno algorithm (67), implemented with the optimx package (68), was used for optimization. *P* values were obtained using Type III Satterthwaite approximations with the lmerTest package (69).

Data Availability. Experiment 2 data are available at https://nda.nih.gov/edit_collection.html?id=2402. Experiment 3 data are available at https://openneuro.org/datasets/ds002372/versions/1.0.0 (46, 47). For inquiries about data in Experiments 1 (33), 4 (48), and 5 (49), readers should contact the original authors.

ACKNOWLEDGMENTS. This work was supported by the Yale Faculty of Arts and Sciences MRI Program, funded by the Office of the Provost and the Department of Psychology; an NSF Graduate Research Fellowship, an American Psychological Association Dissertation Research Award, and a Theresa Seessel Postdoctoral Fellowship (to M.D.R.); NIH Medical Scientist Training Program Training Grant T32GM00720 (to A.S.G.); NSF Grant BCS1558497 (to M.M.C.); and NIH Grants MH108591 (to M.M.C.), EB009666 (to R.T.C.), and T32 DA022975 (to D.S.).

1. P. Seli, E. F. Risko, D. Smilek, D. L. Schacter, Mind-wandering with and without intention. *Trends Cogn. Sci.* **20**, 605–617 (2016).
2. M. Esterman, D. Rothlein, Models of sustained attention. *Curr. Opin. Psychol.* **29**, 174–180 (2019).
3. M. D. Rosenberg, E. S. Finn, R. T. Constable, M. M. Chun, Predicting moment-to-moment attentional state. *Neuroimage* **114**, 249–256 (2015).
4. D. H. Weissman, K. C. Roberts, K. M. Visscher, M. G. Woldorff, The neural bases of momentary lapses in attention. *Nat. Neurosci.* **9**, 971–978 (2006).
5. A. B. Leber, Neural predictors of within-subject fluctuations in attentional control. *J. Neurosci.* **30**, 11458–11465 (2010).
6. K. Christoff, A. M. Gordon, J. Smallwood, R. Smith, J. W. Schooler, Experience sampling during fMRI reveals default network and executive system contributions to mind wandering. *Proc. Natl. Acad. Sci. U.S.A.* **106**, 8719–8724 (2009).
7. F. C. Fortenbaugh, D. Rothlein, R. McGlinchey, J. DeGutis, M. Esterman, Tracking behavioral and neural fluctuations during sustained attention: A robust replication and extension. *Neuroimage* **171**, 148–164 (2018).
8. A. Kucyi, M. Esterman, C. S. Riley, E. M. Valera, Spontaneous default network activity reflects behavioral variability independent of mind-wandering. *Proc. Natl. Acad. Sci. U.S.A.* **113**, 13899–13904 (2016).
9. A. Kucyi *et al.*, Electrophysiological dynamics of antagonistic brain networks reflect attentional fluctuations. *Nat. Commun.* **11**, 325 (2020).
10. A. Kucyi, M. J. Hove, M. Esterman, R. M. Hutchison, E. M. Valera, Dynamic brain network correlates of spontaneous fluctuations in attention. *Cereb. Cortex* **27**, 1831–1840 (2017).
11. J. M. Shine, O. Koyejo, R. A. Poldrack, Temporal metastates are associated with differential patterns of time-resolved connectivity, network topology, and attention. *Proc. Natl. Acad. Sci. U.S.A.* **113**, 9888–9891 (2016).
12. A. Turnbull *et al.*, The ebb and flow of attention: Between-subject variation in intrinsic connectivity and cognition associated with the dynamics of ongoing experience. *Neuroimage* **185**, 286–299 (2019).
13. J. Gonzalez-Castillo *et al.*, Tracking ongoing cognition in individuals using brief, whole-brain functional connectivity patterns. *Proc. Natl. Acad. Sci. U.S.A.* **112**, 8762–8767 (2015).
14. H. Shappell, B. S. Caffo, J. J. Pekar, M. A. Lindquist, Improved state change estimation in dynamic functional connectivity using hidden semi-Markov models. *Neuroimage* **191**, 243–257 (2019).
15. P. Barttfeld *et al.*, Signature of consciousness in the dynamics of resting-state brain activity. *Proc. Natl. Acad. Sci. U.S.A.* **112**, 887–892 (2015).
16. L. J. Larson-Prior *et al.*, Cortical network functional connectivity in the descent to sleep. *Proc. Natl. Acad. Sci. U.S.A.* **106**, 4489–4494 (2009).
17. L. Heine *et al.*, Resting state networks and consciousness: Alterations of multiple resting state network connectivity in physiological, pharmacological, and pathological consciousness States. *Front. Psychol.* **3**, 295 (2012).

18. R. M. Hutchison *et al.*, Dynamic functional connectivity: Promise, issues, and interpretations. *Neuroimage* **80**, 360–378 (2013).
19. J. Gonzalez-Castillo, P. A. Bandettini, Task-based dynamic functional connectivity: Recent findings and open questions. *Neuroimage* **180**, 526–533 (2018).
20. M. G. Preti, T. A. W. Bolton, D. Van De Ville, The dynamic functional connectome: State-of-the-art and perspectives. *Neuroimage* **160**, 41–54 (2017).
21. D. J. Lurie *et al.*, Questions and controversies in the study of time-varying functional connectivity in resting fMRI. *Netw. Neurosci.*, 10.1162/netn_a_00116 (2019).
22. V. D. Calhoun, R. Miller, G. Pearlson, T. Adalı, The chronnectome: Time-varying connectivity networks as the next frontier in fMRI data discovery. *Neuron* **84**, 262–274 (2014).
23. E. S. Finn *et al.*, Functional connectome fingerprinting: Identifying individuals using patterns of brain connectivity. *Nat. Neurosci.* **18**, 1664–1671 (2015).
24. A. S. Greene, S. Gao, D. Scheinost, R. T. Constable, Task-induced brain state manipulation improves prediction of individual traits. *Nat. Commun.* **9**, 2807 (2018).
25. M. Yamashita *et al.*, A prediction model of working memory across health and psychiatric disease using whole-brain functional connectivity. *eLife* **7**, e38844 (2018).
26. E. W. Avery *et al.*, Distributed patterns of functional connectivity predict working memory performance in novel healthy and memory-impaired individuals. *J. Cogn. Neurosci.* **32**, 241–255 (2020).
27. E. M. Galeano Weber, T. Hahn, K. Hilger, C. J. Fiebach, Distributed patterns of occipito-parietal functional connectivity predict the precision of visual working memory. *Neuroimage* **146**, 404–418 (2017).
28. D. Kessler, M. Angstadt, C. Sripada, Growth charting of brain connectivity networks and the identification of attention impairment in youth. *JAMA Psychiatry* **73**, 481–489 (2016).
29. V. N. Poole *et al.*, Intrinsic functional connectivity predicts individual differences in distractibility. *Neuropsychologia* **86**, 176–182 (2016).
30. L. O'Halloran *et al.*, Neural circuitry underlying sustained attention in healthy adolescents and in ADHD symptomatology. *Neuroimage* **169**, 395–406 (2018).
31. M. D. Rosenberg, E. S. Finn, D. Scheinost, R. T. Constable, M. M. Chun, Characterizing attention with predictive network models. *Trends Cogn. Sci.* **21**, 290–302 (2017).
32. K. Yoo *et al.*, Connectome-based predictive modeling of attention: Comparing different functional connectivity features and prediction methods across datasets. *Neuroimage* **167**, 11–22 (2018).
33. M. D. Rosenberg *et al.*, A neuromarker of sustained attention from whole-brain functional connectivity. *Nat. Neurosci.* **19**, 165–171 (2016).
34. M. D. Rosenberg *et al.*, Methylphenidate modulates functional network connectivity to enhance attention. *J. Neurosci.* **36**, 9547–9557 (2016).
35. M. D. Rosenberg, W.-T. Hsu, D. Scheinost, R. Todd Constable, M. M. Chun, Connectome-based models predict separable components of attention in novel individuals. *J. Cogn. Neurosci.* **30**, 160–173 (2018).
36. S. Fountain-Zaragoza, S. Samimy, M. D. Rosenberg, R. S. Prakash, Connectome-based models predict attentional control in aging adults. *Neuroimage* **186**, 1–13 (2019).
37. D. C. Jangraw *et al.*, A functional connectivity-based neuromarker of sustained attention generalizes to predict recall in a reading task. *Neuroimage* **166**, 99–109 (2018).
38. X. Shen *et al.*, Using connectome-based predictive modeling to predict individual behavior from brain connectivity. *Nat. Protoc.* **12**, 506–518 (2017).
39. G. Trapani, C. Altomare, G. Liso, E. Sanna, G. Biggio, Propofol in anesthesia. Mechanism of action, structure-activity relationships, and drug delivery. *Curr. Med. Chem.* **7**, 249–271 (2000).
40. S. S. Patel, K. L. Goa, Sevoflurane. A review of its pharmacodynamic and pharmacokinetic properties and its clinical use in general anaesthesia. *Drugs* **51**, 658–700 (1996).
41. M. Esterman, S. K. Noonan, M. Rosenberg, J. Degutis, In the zone or zoning out? Tracking behavioral and neural fluctuations during sustained attention. *Cereb. Cortex* **23**, 2712–2723 (2013).
42. X. Shen, F. Tokoglu, X. Papademetris, R. T. Constable, Groupwise whole-brain parcellation from resting-state fMRI data for network node identification. *Neuroimage* **82**, 403–415 (2013).
43. M. Krzywinski et al., Circos: An information aesthetic for comparative genomics. *Genome Res.* **19**, 1639–1645 (2009).
44. M. D. Rosenberg, M. M. Chun, "Network models of attention and working memory" in The Cognitive Neurosciences, D. Poeppel, G. R. Mangun, M. S. Gazzaniga, Eds. (MIT Press, ed. 6), in press.
45. M. Chun, Whole brain functional connectivity measures of attention. National Institute of Mental Health Data Archive. https://nda.nih.gov/edit_collection.html?id=2402. Deposited 24 January 2020.
46. M. Salehi *et al.*, There is no single functional atlas even for a single individual: Functional parcel definitions change with task. *Neuroimage* **208**, 116366 (2019).
47. M. Salehi *et al.*, Data from "Yale_Single_Subject_Task_Rest30x." OpenNeuro. https://openneuro.org/datasets/ds002372/versions/1.0.0. Accessed 18 December 2019.
48. M. Qiu, D. Scheinost, R. Ramani, R. T. Constable, Multi-modal analysis of functional connectivity and cerebral blood flow reveals shared and unique effects of propofol in large-scale brain networks. *Neuroimage* **148**, 130–140 (2017).
49. R. Martuzzi, R. Ramani, M. Qiu, N. Rajeevan, R. T. Constable, Functional connectivity and alterations in baseline brain state in humans. *Neuroimage* **49**, 823–834 (2010).
50. O. Miranda-Dominguez *et al.*, Connectotyping: Model based fingerprinting of the functional connectome. *PLoS One* **9**, e111048 (2014).
51. J. Dubois, R. Adolphs, Building a science of individual differences from fMRI. *Trends Cogn. Sci.* **20**, 425–443 (2016).
52. W. R. Shirer, S. Ryali, E. Rykhlevskaia, V. Menon, M. D. Greicius, Decoding subject-driven cognitive states with whole-brain connectivity patterns. *Cereb. Cortex* **22**, 158–165 (2012).
53. J. M. Shine *et al.*, The dynamics of functional brain networks: Integrated network states during cognitive task performance. *Neuron* **92**, 544–554 (2016).
54. A. Kucyi, Just a thought: How mind-wandering is represented in dynamic brain connectivity. *Neuroimage* **180**, 505–514 (2018).
55. A. Kucyi, K. D. Davis, Dynamic functional connectivity of the default mode network tracks daydreaming. *Neuroimage* **100**, 471–480 (2014).
56. S. Noble *et al.*, Influences on the test–retest reliability of functional connectivity mri and its relationship with behavioral utility. *Cereb. Cortex* **27**, 5415–5429 (2017).
57. T. O. Laumann *et al.*, On the stability of BOLD fMRI correlations. *Cereb. Cortex* **27**, 4719–4732 (2017).
58. C. Gratton *et al.*, Functional brain networks are dominated by stable group and individual factors, not cognitive or daily variation. *Neuron* **98**, 439–452.e5 (2018).
59. M. D. Rosenberg, B. J. Casey, A. J. Holmes, Prediction complements explanation in understanding the developing brain. *Nat. Commun.* **9**, 589 (2018).
60. M. Rosenberg, S. Noonan, J. DeGutis, M. Esterman, Sustaining visual attention in the face of distraction: A novel gradual-onset continuous performance task. *Atten. Percept. Psychophys.* **75**, 426–439 (2013).
61. M. Esterman, M. D. Rosenberg, S. K. Noonan, Intrinsic fluctuations in sustained attention and distractor processing. *J. Neurosci.* **34**, 1724–1730 (2014).
62. A. Joshi *et al.*, Unified framework for development, deployment and robust testing of neuroimaging algorithms. *Neuroinformatics* **9**, 69–84 (2011).
63. R. Ciric *et al.*, Benchmarking of participant-level confound regression strategies for the control of motion artifact in studies of functional connectivity. *Neuroimage* **154**, 174–187 (2017).
64. T. Vanderwal, C. Kelly, J. Eilbott, L. C. Mayes, F. X. Castellanos, Inscapes: A movie paradigm to improve compliance in functional magnetic resonance imaging. *Neuroimage* **122**, 222–232 (2015).
65. R. W. Cox, AFNI: Software for analysis and visualization of functional magnetic resonance neuroimages. *Comput. Biomed. Res.* **29**, 162–173 (1996).
66. D. Bates, M. Mächler, B. Bolker, S. Walker, Fitting linear mixed-effects models using lme4. *J. Stat. Softw.*, 10.18637/jss.v067.i01 (2015).
67. R. Byrd, P. Lu, J. Nocedal, C. Zhu, A limited memory algorithm for bound constrained optimization. *SIAM J. Sci. Comput.* **16**, 1190–1208 (1995).
68. J. C. Nash, R. Varadhan, Unifying optimization algorithms to aid software system users: Optimx for R. *J. Stat. Softw.*, 10.18637/jss.v043.i09 (2011).
69. A. Kuznetsova, P. B. Brockhoff, R. H. B. Christensen, lmerTest package: Tests in linear mixed effects models. *J. Stat. Softw.*, 10.18637/jss.v082.i13 (2017).